

PatchRefiner V2: Fast and Lightweight Real-Domain High-Resolution Metric Depth Estimation

Zhenyu Li, Wenqing Cui, Shariq Farooq Bhat, Peter Wonka
King Abdullah University of Science and Technology (KAUST)

<https://zhyever.github.io/patchrefinerv2/>

zhenyu.li.1@kaust.edu.sa

Abstract

While current high-resolution depth estimation methods achieve strong results, they often suffer from computational inefficiencies due to reliance on heavyweight models and multiple inference steps, increasing inference time. To address this, we introduce PatchRefiner V2 (PRV2), which replaces heavy refiner models with lightweight encoders. This reduces model size and inference time but introduces noisy features. To overcome this, we propose a Coarse-to-Fine (C2F) module with a Guided Denoising Unit for refining and denoising the refiner features and a Noisy Pretraining strategy to pretrain the refiner branch to fully exploit the potential of the lightweight refiner branch. Additionally, we introduce a Scale-and-Shift Invariant Gradient Matching (SSIGM) loss to enhance synthetic-to-real domain transfer. PRV2 outperforms state-of-the-art depth estimation methods on UnrealStereo4K in both accuracy and speed, using fewer parameters and faster inference. It also shows improved depth boundary delineation on real-world datasets like CityScape, ScanNet++, and KITTI, demonstrating its versatility across domains.

1. Introduction

Accurate high-resolution depth estimation from a single image is critical for advancements in fields such as autonomous driving, augmented reality, and 3D reconstruction [4, 16, 33, 74]. Current state-of-the-art depth estimation models typically operate at relatively low resolutions (e.g. 0.3 megapixels). High memory requirements, especially at 4K resolution, pose a significant challenge for training depth estimation models that can natively support high-resolution inputs. Recent 4K depth estimation approaches like PatchRefiner [36] (PR) use a tile-based strategy where the high-resolution image is divided into patches. The patch-level depth predictions (fine, local outputs) are then fused with the depth prediction of a downsampled ver-

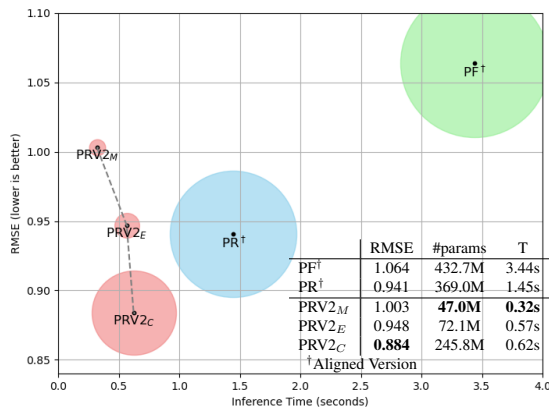


Figure 1. **UnrealStereo4K results.** PatchRefiner V2 (PRV2) significantly outperforms previous high-resolution frameworks. In particular, PRV2_C achieves new SOTA RMSE but being 2.3x faster than PR. PRV2_M is 9.2x smaller and 10.7x faster than PF. PF and PR are short for PatchFusion [34] and PatchRefiner [36], respectively. We present the comparison of PR and PRV2 in Fig. 2.

sion of the input image (coarse, global output) to obtain a single, consistent, high-resolution output.

Despite its success, the PatchRefiner framework faces critical computational efficiency and scalability challenges for real-world applications. It employs the same architecture (a pre-trained base depth model) to extract both global as well as patch-level features. This amounts to at least 17 forward passes of the base model for a single high-resolution input. As the base model used [4, 71, 72] is often large, this results in two major issues: 1) **High inference time** of more than a second per image, and more importantly 2) **High memory requirement**, making the end-to-end training infeasible. Therefore, the PR framework has to adopt stage-wise training, where global and local branches are trained sequentially, leading to a long training time and suboptimal results.

To alleviate these issues, we propose to substitute the large foundational models, such as ZoeDepth [4] or DepthAnything [71, 72], used in the refiner branch [36] with lightweight encoders like MobileNet [24, 51] and EfficientNet [64]. This change significantly reduces the number of parameters and memory usage, decreases inference time, and enables end-to-end training without bells and whistles. However, this modification introduces a trade-off: the model capacity is reduced, and the refiner branch now lacks the depth-aligned feature representation otherwise provided by the previously used pre-trained depth estimation base models. While end-to-end training alleviates some of this limitation, the lack of depth-aligned feature representation remains a concern. Indeed, we observe that the features generated by these lightweight encoders tend to be ‘noisy’ (see Fig. 3) even after ImageNet initialization [13] and end-to-end training. This causes the original Fine-to-Coarse module (F2C) used in PR to struggle to inject rich high-resolution information for the final depth prediction.

We propose two components to improve the feature representation in the refiner branch: 1) The **Coarse-to-fine module (C2F)** which incorporates novel Guided Denoising Units (GDUs) in a bottom-to-top manner [37, 53, 68]. GDUs utilize coarse depth features as guidance to denoise and enhance the high-resolution refiner features. Together with the original Fine-to-Coarse module (F2C), this establishes a bidirectional fusion process: C2F initially denoises and refines high-resolution features using coarse features, followed by F2C’s enhancement of the predicted coarse depth map via residual prediction. 2) **Noisy Pre-training**.¹ Given that the C2F and F2C modules require initialization from scratch, we propose a simple pre-training strategy for the entire refiner branch — including the encoder, C2F, and F2C modules — to enhance feature representation and accelerate learning. During Noisy Pre-training, we replace the input coarse depth features for GDUs with random noise, essentially forcing the refiner branch to learn to extract depth-relevant features from the high-resolution input (Sec. 3.2.3).

Finally, the PR framework [36] employs the Detail and Scale Disentangling (DSD) training strategy to adapt the high-resolution depth estimation framework to real-domain datasets, which enables learning ‘detail’ from synthetic data and ‘scale’ from the real domain. To isolate the scale from the synthetic data, the DSD strategy uses a ranking loss and Scale-and-Shift Invariant (SSI) loss [54]. Motivated by [32], we propose to replace the SSI loss with the Scale-and-Shift Invariant Gradient Matching (SSIGM) loss to learn high-frequency details from the synthetic data directly.

Experiments demonstrate that our advanced framework, **PatchRefiner V2 (PRV2)**, performs effectively across var-

¹We use the term ‘pre-training’ loosely, as this process occurs prior to the final training phase.

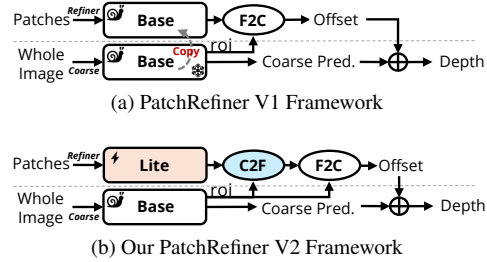


Figure 2. A comparison of (a) PatchRefiner and (b) our proposed PatchRefiner V2. We adopt a lightweight encoder for the refiner branch, which alleviates the inference speed bottleneck, reduces the number of parameters for high-resolution estimation, and facilitates end-to-end training. A novel coarse-to-fine (C2F) module is proposed to denoise features from the lite model and further boost performance.

ious lightweight architectures. As summarized in Fig. 1, PRV2 significantly outperforms other high-resolution metric depth estimation frameworks on the UnrealStereo4K[65] dataset in terms of both quantitative results and inference speed. Additionally, we evaluate the effectiveness of our adopted SSIGM loss across various frameworks (PR and PRV2) on diverse real-world datasets, including CityScene [10] (outdoor, stereo), ScanNet++[73] (indoor, LiDAR and reconstruction), and KITTI[60] (outdoor, LiDAR). Our method reveals significant improvements in depth boundary delineation (e.g., +17.2% boundary F1 on CityScene *w.r.t* [36]) while maintaining accurate scale estimation, showcasing its adaptability and effectiveness across different datasets and domains.

2. Related Work

2.1. High-Resolution Monocular Depth Estimation

Monocular depth estimation (MDE) is a fundamental computer vision task and has recently seen impressive progress with advanced network design [2, 4, 16, 33, 35, 70], supervision [22, 30, 38, 54, 69], formulation [2, 3, 14, 18, 33, 69], training strategy [17, 22, 47, 54], public datasets [10, 11, 21, 55, 62], *etc.* Recently, most SOTA frameworks [4, 26, 71, 72] build on the top of heavy backbones [1, 15, 44, 56], leading to the limitation of low-resolution input. For example, Depth Anything V2 [72] uses ViT-L [15, 44] and can only infer 756×994 (about 0.75 megapixels) images on an NVIDIA V100 32G GPU. While another line of research utilizing the generative model for MDE achieves fine-grained results, a similar dilemma exists. For instance, Marigold [26] based on Stable Diffusion [56] runs with ~0.33 megapixels as default.

This contrasts with the advancements in modern imaging devices, which increasingly capture images at higher resolutions, reflecting the growing demand for high-resolution

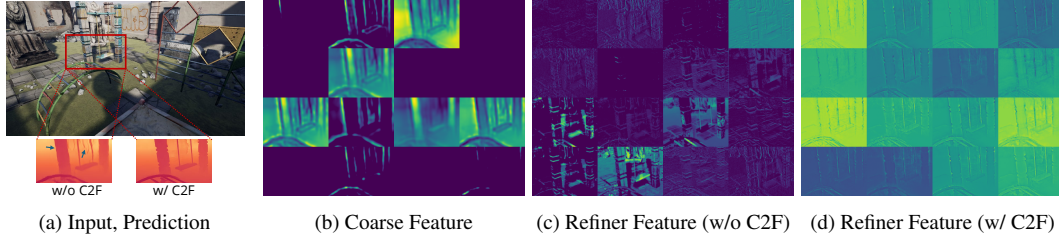


Figure 3. **Visualization of F2C input feature maps.** We showcase the first 16 channels of the F2C input features. (c) Without the C2F module (setting ③ in Tab. 4), the refiner features are ‘noisy’ and hard to interpret. (d) The C2F module helps denoise the refiner features, leading to clear boundaries and better results.

depth estimation [34]. To relax the constraints, initial efforts utilize Guided Depth Super-Resolution (GDSR) [25, 41, 76, 78] and Implicit Functions [8, 43]. Recently, Tile-Based Methods have emerged as an alternative strategy [34, 36, 42], segmenting images into patches for individual estimation before reassembling them into a comprehensive depth map. Since all these methods adopt the dual branch architecture and utilize the same SOTA depth model in both branches, the frameworks are heavy and slow at inference time. By contrast, we aim to achieve fast high-resolution metric depth estimation using the tile-based method with fewer additional parameters.

2.2. Synthetic-to-Real Transfer for MDE

The challenge of collecting high-quality real-domain data for high-resolution depth training has prompted the use of synthetic datasets [36, 52]. Different from traditional methods that utilize the synthetic data within unsupervised domain adaptation frameworks [9, 28, 29, 40, 75, 77], PatchRefiner proposes a more practical setting in which labeled data from both synthetic and real domains is leveraged to improve real-world, high-resolution depth estimation [36]. Motivated by the success of semi-supervised learning [27, 66, 71], they adopt the pseudo-labeling strategy [7, 46, 50, 58, 61] with the Detail and Scale Disentangling (DSD) loss to transfer the fine-grained knowledge learned from the synthetic data to the real domain. However, the adopted scale-and-shift invariant (SSI) loss [54, 71] for detail supervision is indirect and can be ambiguous. This work introduces scale-and-shift invariant *gradient matching* [32] to achieve more effective synthetic-to-real transfer.

3. Method

3.1. Revisiting PatchRefiner V1

We first revisit the PatchRefiner framework [36] (named as PR V1). The PR V1 framework adopts a tile-based approach to address the high memory and computational demands of high-resolution depth estimation [34, 42]. It uti-

lizes a two-step process: (i) Coarse Depth Estimation and (ii) Fine-Grained Depth Refinement, as shown in Fig. 2.

(i) Coarse Depth Estimation: This step involves a coarse depth estimation network, \mathcal{N}_c , which processes downsampled inputs to generate a global depth map, \mathbf{D}_c . This map captures the overall scene structure and provides a baseline for further refinement. Notably, \mathcal{N}_c can be any depth estimation model and is kept fixed after this stage.

(ii) Fine-Grained Depth Refinement: PR introduces a unified refinement network, \mathcal{N}_r , in place of separate fine depth networks and fusion mechanisms [34, 49]. This network refines the coarse depth map by recovering details and enhancing depth precision at a patch level.

The refinement process begins with the cropped input image I , processed by a base depth model \mathcal{N}_d , which shares the same architecture as \mathcal{N}_c . Multi-scale features from both \mathcal{N}_d and \mathcal{N}_c are collected as $\mathcal{F}_d = \{f_d^i\}_{i=1}^L$ and $\tilde{\mathcal{F}}_c = \{\tilde{f}_c^i\}_{i=1}^L$. Following [34], the `roi` [23] operation extracts features from the cropped area as $\tilde{f}_c^i = \text{roi}(f_c^i)$.

These features are then aggregated by a lightweight decoder through concatenation and convolutional blocks, referred to as the Fine-to-Coarse (F2C) module in this paper, which injects fine-grained information into the coarse refinement process. The F2C module constructs the residual depth map \mathbf{D}_r at the input resolution, and the final patch-wise depth map is computed as $\mathbf{D} = \text{roi}(\mathbf{D}_c) + \mathbf{D}_r$.

As the second contribution, PR introduces a teacher-student framework to transfer the fine-grained knowledge learned from the synthetic data to the real domain. The Detail and Scale Disentangling (DSD) loss is designed to help the model balance detail enhancement with scale accuracy by integrating both the scale-consistent ground truth supervision and the detail-focused pseudo labels. Both ranking loss [69] and the scale-and-shift invariant loss [54] can be adopted for pseudo-label supervision.

Limitations of PR V1. Similar to other tile-based methods [34, 49], the PR framework encounters significant challenges with the computational efficiency and scalability for real-world applications due to the shared usage of the base

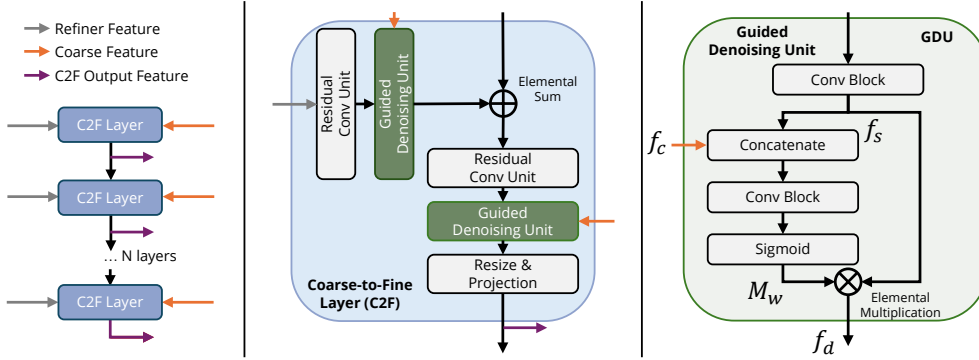


Figure 4. *Left*: Coarse-to-Fine (C2F) module overview. It processes refiner features in a bottom-to-top manner with N successive C2F layers. Each layer is guided by coarse features with corresponding resolution and outputs denoised features for the Fine-to-Coarse (F2C) module. *Center*: C2F layers combine multi-level features with Residual Convolutional Units [37, 54] and denoises the features using Guided Denoising Units (GDU). *Right*: Guidance information from the coarse branch is introduced through a concatenation followed by a convolutional block and then converted to a weight map ranging from 0 to 1 through the sigmoid operator. We then adopt an elementwise multiplication to denoise the shortcut feature.

depth model (e.g., ZoeDepth [4], Depth Anything [71, 72]) across both the coarse and refiner branches. For a given input image, while the coarse branch processes the downsampled image once to gather global information, the refiner branch requires multiple inferences (at least 16 in PR’s default mode) for the patches. Since both branches share the same architecture, the refiner branch becomes the primary efficiency bottleneck. Our goal is to alleviate this bottleneck as much as possible.

Moreover, a heavy framework makes end-to-end training infeasible due to GPU memory limitations. The PR framework has to adopt two stages for training the framework, where global and local branches are trained sequentially. This results in a long training time and suboptimal performance. While the authors claim that multiple-stage training could potentially lead to stage-wise local optima [36], our goal is to pursue end-to-end training.

3.2. PatchRefiner V2 Framework

3.2.1 Lite Framework for Faster Inference and End-to-End Training

We propose a simple solution to address PR V1’s limitations: a lightweight architecture for the refiner branch. Given that the coarse branch already provides a reliable base depth estimation D_c , using the same heavy model for the refiner might be unnecessary. This substitution significantly increases inference speed, reduces the model size, and enables end-to-end training. However, it also results in a noticeable decline in refinement quality compared to previous methods [34, 36]. We attribute this decline to the lack of depth-aligned feature representation in the refiner branch, as shown in Fig. 3.

To compensate for the loss in model capacity and depth-

pretraining by the proposed substitution, we introduce a better architecture design, a Coarse-to-Fine (C2F) Module, and a fast and simple pre-training strategy, Noisy Pretraining (NP).

3.2.2 Coarse-to-Fine Module

Since the refiner branch no longer includes a pretrained depth model, we propose utilizing information from the global coarse branch to guide the selection of relevant details from the fine, patch-level features.

The proposed Coarse-to-Fine (C2F) module shown in Fig. 4 processes the multi-scale features extracted from the lightweight encoder through N successive C2F layers in a bottom-to-up manner [37, 57], mirroring the design of the Fine-to-Coarse (F2C) module [36]. Each C2F layer is designed to progressively enhance and denoise the refiner features with the help of coarse feature representations.

Each layer in the C2F module consists of two components: our proposed Guided Denoising Unit (GDU) and the Residual Convolutional Unit [37, 54]. The GDU introduces coarse feature maps f_c at each stage to refine and denoise the refiner features. Specifically, the coarse features serve as guidance, which are incorporated via the concatenation operation (Cat) followed by the convolutional block (CB). The output of these blocks is passed through a sigmoid activation function (σ) to obtain a weight map M_w , which ranges from 0 to 1. This weight map is then applied to the shortcut features f_s through elemental multiplication \otimes , effectively denoising the shortcut features. This process can be formulated as

$$M_w = \sigma(\text{CB}(\text{Cat}(f_c, f_s))), \quad (1)$$

$$f_d = M_w \otimes f_s, \quad (2)$$

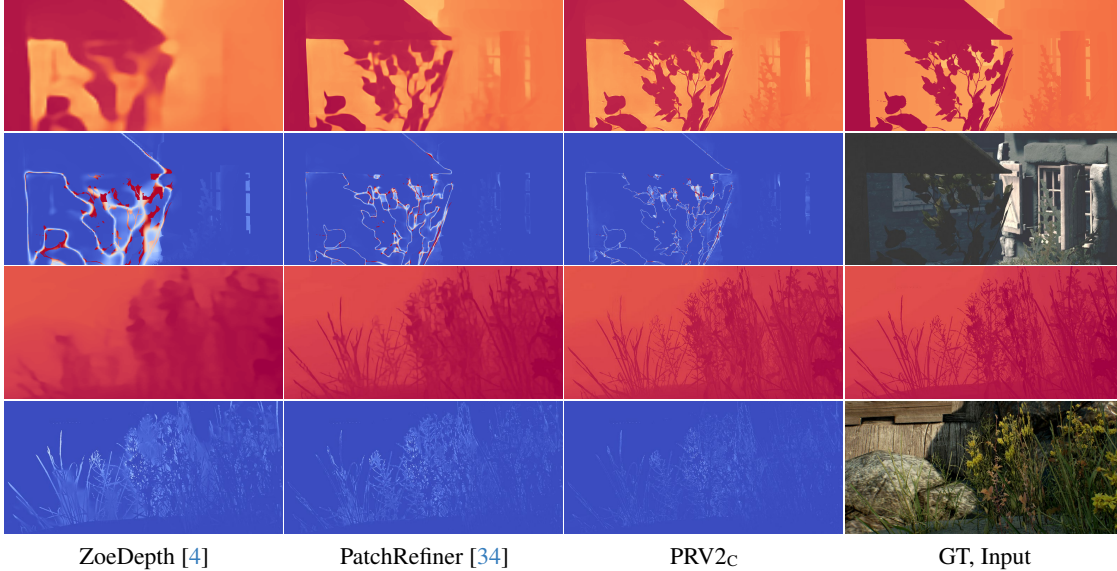


Figure 5. **Qualitative Comparison on UnrealStereo4K.** We show the depth prediction and corresponding error map, respectively. The qualitative comparisons showcased here indicate our PRV2_c outperforms counterparts [4, 36] with sharper edges and lower error around boundaries while achieving faster inference. We show individual patches in all images to emphasize details near depth boundaries.

where the f_d indicates the denoised feature. Associated with the Residual Convolutional Unit, it allows the model to filter out irrelevant noise and enhance the quality of the refined features iteratively across the network layers. After that, we utilize the F2C module to inject the denoised fine-grained information for coarse features, leading to a more effective and better refinement process.

3.2.3 Noisy Pretraining

In PR V1, the framework’s efficacy largely depends on the comprehensive pretraining of the base models in both the coarse and refiner branches [36]. During the subsequent high-resolution training stage, only the Fine-to-Coarse (F2C) module is trained from scratch, representing a minor portion of the overall refiner branch (24.0M vs. 369.0M parameters). In other words, a significant portion (~94%) of the refiner branch is pretrained for depth estimation.

By our substitution, this pretraining is also lost. While the lightweight encoder used can be pretrained on a large-scale dataset with complex strategies, it now constitutes only a small part of the refiner branch (1.3M vs. 47.0M parameters for PRV2_M) and lacks the depth-aligned feature representation. In other words, even if we pre-train the encoder, a significant portion (~98%) of the refiner branch must still be trained from scratch.

To address this issue, we propose a novel approach called Noisy Pretraining (NP). Prior to the high-resolution training, we pretrain the lightweight encoder along with the C2F

and F2C modules. However, a critical aspect of our framework is that both the C2F and F2C modules rely on features from the base model in the coarse branch. These features, however, are challenging to omit during the pretraining process. We propose a straightforward yet effective solution: we randomly generate the coarse features using a normal distribution $N(0, 1)$ as inputs. This forces the refiner branch to learn depth-relevant features without guidance from the coarse branch.

Unlike other strategies [5, 39, 45], which often require careful selection and modification of convolutional layers and their corresponding parameters, our NP method avoids altering the framework’s architecture. As a result, the pretraining and subsequent training stages proceed seamlessly, preserving the integrity of the overall model structure while ensuring that all components of the refiner branch are well-prepared for high-resolution training.

3.3. Scale-and-Shift Invariant Gradient Matching

In the synthetic-to-real transfer stage, PR adopts the scale-and-shift invariant (SSI) loss \mathcal{L}_{ssi} as the pseudo-label supervision as a part of the Detail and Scale Disentangling (DSD) loss \mathcal{L}_{DSD} .

Given a predicted depth d_i and the corresponding pseudo label \hat{d}_i , the SSI loss first aligns them with the least-squares

Method	$\delta_1(\%) \uparrow$	REL \downarrow	RMS \downarrow	SiLog \downarrow	SEE \downarrow	#param \downarrow	T \downarrow	Reference
iDisc [48]	96.940	0.053	1.404	8.502	1.070			ICCV 2023
SMD-Net [65]	97.774	0.044	1.282	7.389	0.883			CVPR 2021
Graph-GDSR [12]	97.932	0.044	1.264	7.469	0.872			CVPR 2022
BoostingDepth [42]	98.104	0.044	1.123	6.662	0.939			CVPR 2021
ZoeDepth [4]	97.717	0.046	1.289	7.448	0.914			-
ZoeDepth+PF [34]	98.419	0.040	1.088	6.212	0.838	432.7M	3.44s	CVPR 2024
ZoeDepth+PF [†] [34]	98.369	0.039	1.064	6.342	0.855			
ZoeDepth+PR [36]	98.821	0.033	0.892	5.417	0.750	369.0M	1.45s	ECCV 2024
ZoeDepth+PR [†] [36]	98.680	0.034	0.941	5.614	0.771			
ZoeDepth+PRV2 _M	98.610	0.034	1.003	5.760	0.832	47.0M	0.32s	Ours
ZoeDepth+PRV2 _E	98.728	0.034	0.948	5.579	0.816	72.1M	0.57s	
ZoeDepth+PRV2 _C	98.863	0.032	0.884	5.281	0.787	245.8M	0.62s	

Table 1. **Quantitative comparison on UnrealStereo4K.** Best results are marked **bold**. PF, PR and PRV2 are short for PatchFusion [34], PatchRefiner [36] and PatchRefiner V2, respectively. We report the $P = 16$ mode for these high-resolution depth estimation frameworks [34]. **Gray lines** present numbers from the original paper with vanilla pretraining settings. [†]: indicates the pretraining aligned version, where we remove the **non-public** Midas pretraining stage [54] adopted for the *fine or refiner branch* in PR and PF to make fair comparisons with our PRV2. The coarse branch is **NOT** modified. #param. and T denote the number of additional parameters adopted for high resolution estimation and the inference time of the *fine or refiner branch* for one input image. Best results are in **bold**.

estimation (LSE) as:

$$(s, t) = \operatorname{argmin}_{s, t} \sum_{i=1}^M (sd_i + t - \hat{d}_i)^2, \quad (3)$$

$$d^* = sd + t, \quad \hat{d}_i^* = \hat{d}_i \quad (4)$$

where the scale s and shift t factors are effectively determined with the closed form [54]. d_i^* and \hat{d}_i^* are scaled and shifted versions of the predicted depth and pseudo label, respectively. Then, a pixel-wise mean absolute error loss is calculated as

$$\mathcal{L}_{ssi} = \frac{1}{M} \sum_{i=1}^M \rho(d_i^* - \hat{d}_i^*), \quad (5)$$

where ρ is the mean absolute error (MAE) loss, and M is the number of pixels. In this paper, we replace the MAE loss with the gradient matching loss [32] that applies a constraint on the gradient variation. It facilitates the model to learn the high-frequency details from the synthetic data directly [32]. We name this combination scale-and-shift invariant gradient matching (SSIGM) loss. It can be formulated as

$$\mathcal{L}_{ssigm} = \frac{1}{M} \sum_{i=1}^M (|\nabla_x R_i| + |\nabla_y R_i|), \quad (6)$$

where $R_i = \hat{d}_i - \hat{d}_i^*$. Similar to PR [36], we utilize λ to control the strength of pseudo-label supervision.

Method	$\delta_1(\%) \uparrow$	RMS \downarrow	SEE \downarrow
Depth Anything V2 (DAV2) [72]	98.072	1.144	0.908
DAV2+PRV2 _M	98.771	0.919	0.813
DAV2+PRV2 _E	98.874	0.869	0.784
DAV2+PRV2 _C	98.929	0.859	0.779

Table 2. **Framework performance with Depth Anything V2 as the base model on UnrealStereo4K.** Our advanced framework can consistently boost the SoTA depth estimator for high-resolution metric depth estimation.

4. Experiments

4.1. Datasets and Metrics

Datasets: We evaluate the effectiveness of our proposed framework on the UnrealStereo4K dataset [65] (Synthetic), which offers synthetic stereo images at a 4K resolution (2160×3840), each paired with accurate, boundary-complete pixel-wise ground truth. Adhering to the dataset splits in [34, 36, 65], we employ a default patch size of 540×960 for compatibility with [34, 36]. In terms of the synthetic-to-real transfer part, we use the Cityscapes [10] (Real, Stereo), ScanNet++ (Real, LiDAR, Reconstruction), and KITTI (Real, LiDAR) datasets. Since the Cityscapes dataset offers a comprehensive suite of urban scene images, segmentation masks, and disparity maps at a relatively high resolution, we conduct comparison experiments on the Cityscapes dataset and provide qualitative comparison results on ScanNet++ and KITTI datasets. More details about datasets are provided in *supplementary materials*.

²https://github.com/zhyever/PatchRefiner/blob/main/docs/user_training.md

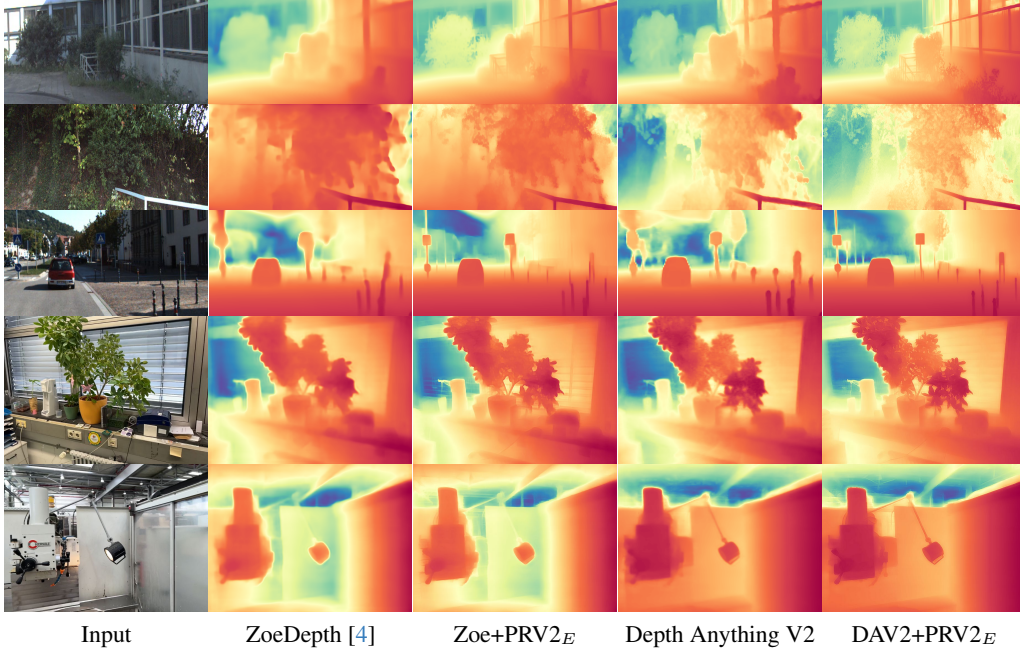


Figure 6. **Qualitative Comparison on KITTI and ScanNet++.** Our PVR2 can consistently boost high-resolution depth estimation with various base models (ZoeDepth, DAV2) on various real-domain datasets. Zoom in to better perceive details near boundaries.

Method	Data		pl gen	Scale			Boundary		
	S	\mathcal{R}		$\delta_1(\%) \uparrow$	REL \downarrow	RMS \downarrow	EdgeAcc \downarrow	EdgeComp \downarrow	F1 \uparrow
ZoeDepth [4]		✓	-	92.214	0.081	9.097	3.62	42.18	19.15
ZoeDepth [4] + FT	✓	✓	-	92.249	0.081	9.092	3.61	38.69	20.02
PR (zero-shot) [36]	✓		-	3.630	0.436	24.506	3.25	9.16	31.10
PR [36]		✓	-	93.295	0.076	8.324	3.39	22.14	26.99
PR + Ranking [36]	✓	✓	online	93.308	0.076	8.313	3.28	17.65	29.53
PR + SSI [36]	✓	✓	online	93.300	0.075	8.313	3.25	17.11	30.02
PR + SSIGM (Ours)	✓	✓	online	93.277	0.076	8.315	3.00	15.47	35.19
PR + SSIGM (Ours)	✓	✓	offline	93.320	0.076	8.297	<u>3.03</u>	14.70	34.89
PRV2 _E		✓	-	93.023	0.076	8.513	3.29	22.60	27.98
PRV2 _E + Ranking [36]	✓	✓	online	92.905	0.077	8.533	3.30	21.72	28.27
PRV2 _E + SSI [36]	✓	✓	online	92.901	0.076	8.533	3.24	21.12	29.22
PRV2 _E + SSIGM (Ours)	✓	✓	online	92.883	0.077	8.534	3.04	17.78	35.32
PRV2 _E + SSIGM (Ours)	✓	✓	offline	92.889	0.077	8.530	<u>3.10</u>	16.97	<u>34.85</u>

Table 3. **Quantitative comparison on CityScapes.** FT is short for fine-tuning. We mainly compare our proposed SSIGM loss with the ranking [69] and scale-and-shift loss [54, 71] adopted in [36]. Reported results are from the official implementation². Best boundary results are in **bold**, second best are underlined for each different framework.

Metrics: Following [34, 36], we adopt standard depth evaluation metrics from [4, 16, 48] and the Soft Edge Error (SEE) from [6, 34, 65] for *scale* evaluation. As for the *boundary* evaluation on the real-domain datasets (Cityscapes), we adopt the standard protocol introduced in [36] and utilize the F1 score, Edge Accuracy, and Edge Completeness metrics to evaluate the boundary quality.

4.2. Implementation Details

PRV2 on Synthetic Dataset: For training on the synthetic dataset, we employ the scale-invariant log loss \mathcal{L}_{silog} , as introduced in [2, 16, 31]. We initialize the coarse network

\mathcal{N}_c with pretrained weights from the NYU-v2 dataset [62], adhering to the approach in [34, 36] for a fair comparison. As for the refiner branch, we employ the MobileNet-Small [51], EfficientNet-B5 [64], and Convnext-Large for PRV2_M, PRV2_E, and PRV2_C, respectively. We perform the noisy pretraining for the refiner branch for 96 epochs. The \mathcal{N}_c is independently trained for 24 epochs and fine-tuned with the refiner branch in a fully end-to-end manner for another 48 epochs on the synthetic dataset. During inference, we implement Consistency-Aware Inference, as described in [34], to optimize performance.

Learning on Real-Domain Dataset: Following [36], we

first train the entire framework on the target real-domain dataset with the same setting as the synthetic dataset. After that, we fine-tune the model with the Detail and Scale Disentangling loss for two epochs to refine depth estimations. To achieve a fair comparison with PR, we use the ZoeDepth+PR and DepthAnything V2+PR as the teacher model to generate pseudo labels for our ZoeDepth+PRV2 and DepthAnything V2+PRV2 models, respectively.

4.3. Main Results

Synthetic Dataset: As shown in Tab. 1, our most lightweight model, PRV2_M, not only improves RMSE by 22.2% compared to the base depth model but is also 9.2x smaller and 10.7x faster than PatchFusion (PF) in terms of parameter count and inference speed, respectively. Our middleweight model, PRV2_E, achieves comparable RMSE to the previous SoTA PR while being 2.5x faster and 5.1x smaller, offering an excellent balance between performance and efficiency. With ConvNext as the backbone, PRV2_C sets a new SoTA with an RMSE of 0.884, while being 2.3x faster than PR. Qualitative results in Fig. 5 demonstrate PRV2_C's superior boundary delineation. Furthermore, when using Depth Anything V2 as the base model, as shown in Tab. 2, our framework consistently boosts performance across different lightweight refiner models, highlighting its versatility.

Real-Domain Dataset: Tab. 3 and Fig. 6 illustrate the performance gains achieved with our proposed SSIGM loss. While maintaining a comparable scale RMSE to the Ranking and SSI losses used in [36], SSIGM significantly improves boundary F1 scores, with gains of 17.2% for PR and 20.9% for PRV2_E. Remarkably, the boundary F1 scores even surpass those achieved during zero-shot inference, demonstrating the model's strong ability to predict accurate depth at object boundaries. Additionally, we evaluate different methods for generating pseudo labels. Although the offline approach shows similar performance, it eliminates the need for forward passes through the teacher model during training.

4.4. Ablation Studies and Discussion

We ablate and discuss the contributions of individual components proposed for PRV2. We employ the MobileNet in the refiner branch and adopt $P = 16$ patches for clarity and ease of comparison. The inference time benchmarks are performed on a single NVIDIA A100 GPU.

Framework Design: As shown in Tab. 4, we start with a baseline framework (①) in which we only substitute the base depth model in the refiner branch in PR with the lightweight encoder. While the inference time and model size are drastically reduced, quality is also degraded by a large margin. Simply adding more parameters to scale up the F2C cannot improve the performance, as shown in ②.

	Method				RMSE	#param.	T(s)
	Coarse Baseline				1.289	-	-
	F2C	E2E	C2F	NP			
①	✓				1.201	27.5M	0.08s
②	✓				1.214	70.2M	0.38s
③	✓	✓			1.184	27.5M	0.08s
④	✓	✓	✓		1.041	47.0M	0.32s
★	✓	✓	✓	✓	1.003	47.0M	0.32s
⑥	w/o GDU				1.137	34.5M	0.19s
⑦	replace GDU with PatchRefiner fusion				1.202	47.0M	0.32s
⑧	AP, only load encoder				1.029	47.0M	0.32s
⑨	w/o ImageNet pretraining				1.059	47.0M	0.32s

Table 4. **Ablation study of the framework on UnrealStereo4K.** F2C and C2F denote the fine-to-coarse and coarse-to-fine module in the bi-directional fusion module, respectively. E2E and NP are short for end-to-end training and noisy pretraining. Time: average inference time of the refiner branch for one image.

Adopting an end-to-end training strategy can help improve the model performance (③). With the help of our proposed C2F that denoises the refiner features effectively, as shown in Fig. 3, the model's RMSE is reduced by 12.2% while only introducing a satisfactory overhead (③, ④). We also adopt different variants for C2F to evaluate the effectiveness. Firstly, we remove the GDU so that the C2F degrades to a simple bottom-to-top aggregation module (⑥). While it can still improve the model performance, there is a large margin compared with the complete C2F module. Then, we replace the GDU with the fusion module used in F2C (⑦). This results in a significant drop in performance. We argue this is due to the coarse features dominating the fusion process. The high-frequency information cannot be preserved correctly, leading to a performance on par with ①.

Noisy Pretraining: When equipped with the NP (★), our model achieves the best performance with 22.2% improvement over the coarse baseline in terms of RMSE. To prove our claim in the method section, we conduct the experiment by only loading the encoder part parameters after the NP process (⑧). The discrepancy in performance indicates that the pretraining of C2F and F2C modules is also crucial for the model performance, which is often ignored in the current depth estimation community. Then, we discard the ImageNet [13] pretrained parameters for the lightweight encoder and train the entire refiner branch from scratch (⑨). The result validates our assumption that merely pretraining the encoder is not enough for better performance due to the lack of depth-aligned representation.

5. Conclusion

We presented **PatchRefiner V2**, an enhanced and efficient framework for high-resolution monocular metric depth estimation. Building on the strengths of the original PatchRefiner, PRV2 introduces a lightweight refiner branch, dramatically improving inference speed and re-

ducing model size. With the novel Coarse-to-Fine (C2F) module and Noisy Pretraining strategy, our framework successfully mitigates the challenges posed by noisy features and the lack of pre-training of the refiner branch. Furthermore, we introduced the Scale-and-Shift Invariant Gradient Matching (SSIGM) loss to enhance boundary accuracy and improve synthetic-to-real transfer. Our framework significantly outperforms previous methods on the UnrealStereo4K dataset, achieving up to 9.2x fewer parameters and 10.7x faster inference. PRV2 also demonstrates considerable improvements in depth boundary delineation on real-world datasets like CityScape, ScanNet++, and KITTI, showcasing its adaptability and effectiveness across different domains and base models.

A. Dataset

UnrealStereo4K (Synthetic, 4K): The UnrealStereo4K dataset [65] consists of synthetic stereo images with a resolution of 2160×3840 pixels, each paired with precise, boundary-complete pixel-wise ground truth. Images with labeling inaccuracies are excluded based on the Structural Similarity Index (SSIM) [67], a process adapted from [34, 36]. Ground truth depth maps are computed from the provided disparity maps using specific camera parameters. Consistent with the splits suggested in [34, 36, 65], the experiments utilize a patch size of 540×960 pixels for fair comparison.

CityScapes (Real, Stereo): The CityScapes dataset [10] provides a diverse collection of urban scene images, segmentation masks, and disparity maps at a resolution of 1024×2048 pixels. This dataset surpasses many in its domain in terms of image density, volume, and resolution [59, 60, 62, 63]. For our experiments, we use a standard patch size of 256×512 pixels, primarily focusing on this dataset for testing our models following [36].

ScanNet++ (Real, LiDAR, Reconstruction): ScanNet++ [73] is an expansive dataset featuring high-resolution indoor images (1440×1920 pixels), low-resolution depth maps from iPhone LiDAR sensors (192×256 pixels), and high-resolution depth maps derived from laser scan reconstructions (1440×1920 pixels). The low-resolution depth maps are employed during the training phase following [36], with a selected patch size of 720×960 pixels to accommodate the high-resolution setup.

KITTI (Real, LiDAR): The KITTI dataset [20] includes stereo images and corresponding 3D laser scans of outdoor scenes, captured using equipment mounted on a moving vehicle. The RGB images are captured at a resolution of 376×1241 pixels, paired with sparse ground truth depth maps. Adhering to the widely-used Eigen split [16], we employ approximately 26,000 images from the left camera for training and 697 frames for testing. In line with the methodology of Garg et al. [19], the images and depth maps are

Method	EdgeAcc↓	EdgeComp↓
SSI Loss [36, 54, 71]	3.28	17.04
GM Loss [32]	3.00	15.48
GMSSI Loss	3.25	<u>14.89</u>
SSIGM Loss (Ours)	<u>3.03</u>	14.70

Table 5. **Ablation study of the loss design on CityScapes.** GMSSI indicates that we first calculate the gradient map of the prediction and pseudo label, align them via LSE, and then calculate the scale-and-shift invariant loss.

	Method				RMSE	#param.	T(s)
	Coarse Baseline				1.289	-	-
	F2C	E2E	C2F	NP			
①	✓				1.118	51.7M	0.29s
②	✓				1.185	95.6M	0.47s
③	✓	✓			1.100	51.7M	0.29s
④	✓	✓	✓		0.985	72.1M	0.57s
★	✓	✓	✓	✓	0.947	72.1M	0.57s

Table 6. **Ablation study of PRV2_E on UnrealStereo4K.** F2C and C2F denote the fine-to-coarse and coarse-to-fine module in the bi-directional fusion module, respectively. E2E and NP are short for end-to-end training and noisy pretraining. Time: average inference time of the refiner branch for one image.

	Method				RMSE	#param.	T(s)
	Coarse Baseline				1.289	-	-
	F2C	E2E	C2F	NP			
①	✓				1.095	226.9M	0.38s
②	✓				1.151	270.9M	0.61s
③	✓	✓			1.089	226.9M	0.38s
④	✓	✓	✓		0.946	245.8M	0.62s
★	✓	✓	✓	✓	0.883	245.8M	0.62s

Table 7. **Ablation study of PRV2_C on UnrealStereo4K.**

cropped to a resolution of 352×1216 pixels for evaluation purposes, with a patch size of 176×304 pixels used across the KITTI experiments.

B. Ablation Study

Synthetic-to-Real Transfer: We ablate the SSIGM loss on the CityScapes dataset and utilize the offline manner to generate pseudo labels. To achieve fair comparison with PatchRefiner (PRV1) [36], we apply various types of losses on the vanilla PRV1 framework instead of the advanced PRV2 in this ablation study. As shown in Tab. 5, directly adopting the gradient matching loss can significantly boost the boundary metric. Combining the SSI and GM losses can combine the best of both worlds. Our experiments also indicate that the order of combination matters for a better trade-off. First adopting the scale-and-shift alignment and then applying the gradient matching works better compared with the reversed one (GMSSI).

Framework Design: We present more ablation studies

about framework design based on PRV2_E and PRV2_C as shown in Tab. 6 and Tab. 7, respectively. we start with a baseline framework (①) in which we only substitute the base depth model in the refiner branch in PR with the lightweight encoder. While the inference time and model size are drastically reduced, quality is also degraded. Simply adding more parameters to scale up the F2C cannot improve the performance, as shown in ②. Adopting an end-to-end training strategy can help improve the model performance (③). With the help of our proposed C2F that denoises the refiner features effectively, the model’s RMSE is reduced while only introducing a satisfactory overhead (③, ④). When equipped with the NP (★), our model achieves the best performance.

References

- [1] Hangbo Bao, Li Dong, Songhao Piao, and Furu Wei. Beit: Bert pre-training of image transformers. *arXiv preprint arXiv:2106.08254*, 2021. 2
- [2] Shariq Farooq Bhat, Ibraheem Alhashim, and Peter Wonka. Adabins: Depth estimation using adaptive bins. In *CVPR*, pages 4009–4018, 2021. 2, 7
- [3] Shariq Farooq Bhat, Ibraheem Alhashim, and Peter Wonka. Localbins: Improving depth estimation by learning local distributions. In *European Conference on Computer Vision*, pages 480–496. Springer, 2022. 2
- [4] Shariq Farooq Bhat, Reiner Birkel, Diana Wofk, Peter Wonka, and Matthias Müller. Zoedepth: Zero-shot transfer by combining relative and metric depth. *arXiv preprint arXiv:2302.12288*, 2023. 1, 2, 4, 5, 6, 7
- [5] Tim Brooks, Aleksander Holynski, and Alexei A Efros. Instructpix2pix: Learning to follow image editing instructions. In *CVPR*, pages 18392–18402, 2023. 5
- [6] Chuangrong Chen, Xiaozhi Chen, and Hui Cheng. On the over-smoothing problem of cnn based disparity estimation. In *ICCV*, pages 8997–9005, 2019. 7
- [7] Chaoqi Chen, Weiping Xie, Wenbing Huang, Yu Rong, Xinghao Ding, Yue Huang, Tingyang Xu, and Junzhou Huang. Progressive feature alignment for unsupervised domain adaptation. In *CVPR*, pages 627–636, 2019. 3
- [8] Yinbo Chen, Sifei Liu, and Xiaolong Wang. Learning continuous image representation with local implicit image function. In *CVPR*, pages 8628–8638, 2021. 3
- [9] Yun-Chun Chen, Yen-Yu Lin, Ming-Hsuan Yang, and Jia-Bin Huang. Crdoco: Pixel-level domain transfer with cross-domain consistency. In *CVPR*, pages 1791–1800, 2019. 3
- [10] Marius Cordts, Mohamed Omran, Sebastian Ramos, Timo Rehfeld, Markus Enzweiler, Rodrigo Benenson, Uwe Franke, Stefan Roth, and Bernt Schiele. The cityscapes dataset for semantic urban scene understanding. In *CVPR*, pages 3213–3223, 2016. 2, 6, 9
- [11] Angela Dai, Angel X Chang, Manolis Savva, Maciej Halber, Thomas Funkhouser, and Matthias Nießner. Scannet: Richly-annotated 3d reconstructions of indoor scenes. In *CVPR*, pages 5828–5839, 2017. 2
- [12] Riccardo De Lutio, Alexander Becker, Stefano D’Aronco, Stefania Russo, Jan D Wegner, and Konrad Schindler. Learning graph regularisation for guided super-resolution. In *CVPR*, pages 1979–1988, 2022. 6
- [13] Jia Deng, Wei Dong, Richard Socher, Li-Jia Li, Kai Li, and Li Fei-Fei. Imagenet: A large-scale hierarchical image database. In *CVPR*, pages 248–255. Ieee, 2009. 2, 8
- [14] Raul Diaz and Amit Marathe. Soft labels for ordinal regression. In *CVPR*, pages 4738–4747, 2019. 2
- [15] Alexey Dosovitskiy, Lucas Beyer, Alexander Kolesnikov, Dirk Weissenborn, Xiaohua Zhai, Thomas Unterthiner, Mostafa Dehghani, Matthias Minderer, Georg Heigold, Sylvain Gelly, et al. An image is worth 16x16 words: Transformers for image recognition at scale. *arXiv preprint arXiv:2010.11929*, 2020. 2
- [16] David Eigen, Christian Puhrsch, and Rob Fergus. Depth map prediction from a single image using a multi-scale deep network. *NeurIPS*, 27, 2014. 1, 2, 7, 9
- [17] Rizhao Fan, Matteo Poggi, and Stefano Mattoccia. Contrastive learning for depth prediction. In *CVPRW*, pages 3225–3236, 2023. 2
- [18] Huan Fu, Mingming Gong, Chaohui Wang, Kayhan Batmanghelich, and Dacheng Tao. Deep ordinal regression network for monocular depth estimation. In *CVPR*, pages 2002–2011, 2018. 2
- [19] Ravi Garg, Vijay Kumar Bg, Gustavo Carneiro, and Ian Reid. Unsupervised cnn for single view depth estimation: Geometry to the rescue. In *Computer Vision–ECCV 2016: 14th European Conference, Amsterdam, The Netherlands, October 11–14, 2016, Proceedings, Part VIII 14*, pages 740–756. Springer, 2016. 9
- [20] Andreas Geiger, Philip Lenz, and Raquel Urtasun. Are we ready for autonomous driving? the kitti vision benchmark suite. In *CVPR*, pages 3354–3361. IEEE, 2012. 9
- [21] Andreas Geiger, Philip Lenz, Christoph Stiller, and Raquel Urtasun. Vision meets robotics: The kitti dataset. *IJRR*, 32(11):1231–1237, 2013. 2
- [22] Clément Godard, Oisín Mac Aodha, Michael Firman, and Gabriel J Brostow. Digging into self-supervised monocular depth estimation. In *ICCV*, pages 3828–3838, 2019. 2
- [23] Kaiming He, Georgia Gkioxari, Piotr Dollár, and Ross Girshick. Mask r-cnn. In *ICCV*, pages 2961–2969, 2017. 3
- [24] Andrew Howard, Mark Sandler, Grace Chu, Liang-Chieh Chen, Bo Chen, Mingxing Tan, Weijun Wang, Yukun Zhu, Ruoming Pang, Vijay Vasudevan, et al. Searching for mobilenetv3. In *CVPR*, pages 1314–1324, 2019. 2
- [25] Tak-Wai Hui, Chen Change Loy, and Xiaoou Tang. Depth map super-resolution by deep multi-scale guidance. In *ECCV*, pages 353–369. Springer, 2016. 3
- [26] Bingxin Ke, Anton Obukhov, Shengyu Huang, Nando Metzger, Rodrigo Caye Daudt, and Konrad Schindler. Repurposing diffusion-based image generators for monocular depth estimation. In *CVPR*, pages 9492–9502, 2024. 2
- [27] Alexander Kirillov, Eric Mintun, Nikhila Ravi, Hanzi Mao, Chloe Rolland, Laura Gustafson, Tete Xiao, Spencer Whitehead, Alexander C Berg, Wan-Yen Lo, et al. Segment anything. In *ICCV*, pages 4015–4026, 2023. 3

- [28] PNRV Koutilya, Hao Zhou, and David Jacobs. Sharingan: Combining synthetic and real data for unsupervised geometry estimation. In *CVPR*, page 5, 2020. 3
- [29] Jogendra Nath Kundu, Phani Krishna Uppala, Anuj Pahuja, and R Venkatesh Babu. Adadepth: Unsupervised content congruent adaptation for depth estimation. In *CVPR*, pages 2656–2665, 2018. 3
- [30] Jae-Han Lee and Chang-Su Kim. Multi-loss rebalancing algorithm for monocular depth estimation. In *ECCV*, pages 785–801. Springer, 2020. 2
- [31] Jin Han Lee, Myung-Kyu Han, Dong Wook Ko, and Il Hong Suh. From big to small: Multi-scale local planar guidance for monocular depth estimation. *arXiv preprint arXiv:1907.10326*, 2019. 7
- [32] Zhengqi Li and Noah Snavely. Megadepth: Learning single-view depth prediction from internet photos. In *CVPR*, pages 2041–2050, 2018. 2, 3, 6, 9
- [33] Zhenyu Li, Xuyang Wang, Xianming Liu, and Junjun Jiang. Binsformer: Revisiting adaptive bins for monocular depth estimation. *arXiv preprint arXiv:2204.00987*, 2022. 1, 2
- [34] Zhenyu Li, Shariq Farooq Bhat, and Peter Wonka. Patchfusion: An end-to-end tile-based framework for high-resolution monocular metric depth estimation. *arXiv preprint arXiv:2312.02284*, 2023. 1, 3, 4, 5, 6, 7, 9
- [35] Zhenyu Li, Zehui Chen, Xianming Liu, and Junjun Jiang. Depthformer: Exploiting long-range correlation and local information for accurate monocular depth estimation. *Machine Intelligence Research*, pages 1–18, 2023. 2
- [36] Zhenyu Li, Shariq Farooq Bhat, and Peter Wonka. Patchrefiner: Leveraging synthetic data for real-domain high-resolution monocular metric depth estimation. *arXiv preprint arXiv:2406.06679*, 2024. 1, 2, 3, 4, 5, 6, 7, 8, 9
- [37] Guosheng Lin, Anton Milan, Chunhua Shen, and Ian Reid. Refinenet: Multi-path refinement networks for high-resolution semantic segmentation. In *CVPR*, pages 1925–1934, 2017. 2, 4
- [38] Ce Liu, Suryansh Kumar, Shuhang Gu, Radu Timofte, and Luc Van Gool. Single image depth prediction made better: A multivariate gaussian take. In *CVPR*, pages 17346–17356, 2023. 2
- [39] Ruoshi Liu, Rundi Wu, Basile Van Hoorick, Pavel Tokmakov, Sergey Zakharov, and Carl Vondrick. Zero-1-to-3: Zero-shot one image to 3d object. In *ICCV*, pages 9298–9309, 2023. 5
- [40] Adrian Lopez-Rodriguez and Krystian Mikołajczyk. Desc: Domain adaptation for depth estimation via semantic consistency. *International Journal of Computer Vision*, 131(3): 752–771, 2023. 3
- [41] Nando Metzger, Rodrigo Caye Daudt, and Konrad Schindler. Guided depth super-resolution by deep anisotropic diffusion. In *CVPR*, pages 18237–18246, 2023. 3
- [42] S Mahdi H Miangoleh, Sebastian Dille, Long Mai, Sylvain Paris, and Yagiz Aksoy. Boosting monocular depth estimation models to high-resolution via content-adaptive multi-resolution merging. In *CVPR*, pages 9685–9694, 2021. 3, 6
- [43] Ben Mildenhall, Pratul P Srinivasan, Matthew Tancik, Jonathan T Barron, Ravi Ramamoorthi, and Ren Ng. Nerf: Representing scenes as neural radiance fields for view synthesis. *Communications of the ACM*, 65(1):99–106, 2021. 3
- [44] Maxime Oquab, Timothée Darcet, Théo Moutakanni, Huy Vo, Marc Szafraniec, Vasil Khalidov, Pierre Fernandez, Daniel Haziza, Francisco Massa, Alaaeldin El-Nouby, et al. Dinov2: Learning robust visual features without supervision. *arXiv preprint arXiv:2304.07193*, 2023. 2
- [45] Ege Ozguroglu, Ruoshi Liu, Dídac Surís, Dian Chen, Achal Dave, Pavel Tokmakov, and Carl Vondrick. pix2gestalt: Amodal segmentation by synthesizing wholes. In *CVPR*, pages 3931–3940. IEEE Computer Society, 2024. 5
- [46] Giuseppe Pastore, Fabio Cermelli, Yongqin Xian, Massimiliano Mancini, Zeynep Akata, and Barbara Caputo. A closer look at self-training for zero-label semantic segmentation. In *CVPR*, pages 2693–2702, 2021. 3
- [47] Andra Petrovai and Sergiu Nedevschi. Exploiting pseudo labels in a self-supervised learning framework for improved monocular depth estimation. In *CVPR*, pages 1578–1588, 2022. 2
- [48] Luigi Piccinelli, Christos Sakaridis, and Fisher Yu. idisc: Internal discretization for monocular depth estimation. In *CVPR*, pages 21477–21487, 2023. 6, 7
- [49] Florentin Poucin, Andrea Kraus, and Martin Simon. Boosting instance segmentation with synthetic data: A study to overcome the limits of real world data sets. In *Int. Conf. Comput. Vis. Worksh.*, pages 945–953, 2021. 3
- [50] Dong-Hyun Lee Pseudo-Label. The simple and efficient semi-supervised learning method for deep neural networks. In *ICML 2013 Workshop: Challenges in Representation Learning*, pages 1–6, 2013. 3
- [51] Danfeng Qin, Chas Lechner, Manolis Delakis, Marco Fornoni, Shixin Luo, Fan Yang, Weijun Wang, Colby Banbury, Chengxi Ye, Berkin Akin, et al. Mobilenetv4-universal models for the mobile ecosystem. *arXiv preprint arXiv:2404.10518*, 2024. 2, 7
- [52] Aakash Rajpal, Noshaba Cheema, Klaus Illgner-Fehns, Philipp Slusallek, and Sunil Jaiswal. High-resolution synthetic rgb-d datasets for monocular depth estimation. In *CVPR*, pages 1188–1198, 2023. 3
- [53] René Ranftl, Alexey Bochkovskiy, and Vladlen Koltun. Vision transformers for dense prediction. In *ICCV*, pages 12179–12188, 2021. 2
- [54] René Ranftl, Katrin Lasinger, David Hafner, Konrad Schindler, and Vladlen Koltun. Towards robust monocular depth estimation: Mixing datasets for zero-shot cross-dataset transfer. *IEEE TPAMI*, 44(3), 2022. 2, 3, 4, 6, 7, 9
- [55] Mike Roberts, Jason Ramapuram, Anurag Ranjan, Atulit Kumar, Miguel Angel Bautista, Nathan Paczan, Russ Webb, and Joshua M Susskind. Hypersim: A photorealistic synthetic dataset for holistic indoor scene understanding. In *ICCV*, pages 10912–10922, 2021. 2
- [56] Robin Rombach, Andreas Blattmann, Dominik Lorenz, Patrick Esser, and Björn Ommer. High-resolution image synthesis with latent diffusion models. In *CVPR*, pages 10684–10695, 2022. 2

- [57] Olaf Ronneberger, Philipp Fischer, and Thomas Brox. U-net: Convolutional networks for biomedical image segmentation, 2015. [4](#)
- [58] Kuniaki Saito, Yoshitaka Ushiku, and Tatsuya Harada. Asymmetric tri-training for unsupervised domain adaptation. In *International Conference on Machine Learning*, pages 2988–2997. PMLR, 2017. [3](#)
- [59] Daniel Scharstein, Heiko Hirschmüller, York Kitajima, Greg Krathwohl, Nera Nešić, Xi Wang, and Porter Westling. High-resolution stereo datasets with subpixel-accurate ground truth. In *Pattern Recognition: 36th German Conference, GCPR 2014, Münster, Germany, September 2-5, 2014, Proceedings 36*, pages 31–42. Springer, 2014. [9](#)
- [60] Thomas Schops, Johannes L Schonberger, Silvano Galliani, Torsten Sattler, Konrad Schindler, Marc Pollefeys, and Andreas Geiger. A multi-view stereo benchmark with high-resolution images and multi-camera videos. In *CVPR*, pages 3260–3269, 2017. [2](#), [9](#)
- [61] Inkyu Shin, Yi-Hsuan Tsai, Bingbing Zhuang, Samuel Schulter, Buyu Liu, Sparsh Garg, In So Kweon, and Kuk-Jin Yoon. Mm-tta: multi-modal test-time adaptation for 3d semantic segmentation. In *CVPR*, pages 16928–16937, 2022. [3](#)
- [62] Nathan Silberman, Derek Hoiem, Pushmeet Kohli, and Rob Fergus. Indoor segmentation and support inference from rgb-d images. In *ECCV*, pages 746–760. Springer, 2012. [2](#), [7](#), [9](#)
- [63] Shuran Song, Samuel P Lichtenberg, and Jianxiong Xiao. Sun rgb-d: A rgb-d scene understanding benchmark suite. In *CVPR*, pages 567–576, 2015. [9](#)
- [64] Mingxing Tan and Quoc V. Le. Efficientnet: Rethinking model scaling for convolutional neural networks. *CoRR*, abs/1905.11946, 2019. [2](#), [7](#)
- [65] Fabio Tosi, Yiyi Liao, Carolin Schmitt, and Andreas Geiger. Smd-nets: Stereo mixture density networks. In *CVPR*, pages 8942–8952, 2021. [2](#), [6](#), [7](#), [9](#)
- [66] Jesper E Van Engelen and Holger H Hoos. A survey on semi-supervised learning. *Machine learning*, 109(2):373–440, 2020. [3](#)
- [67] Zhou Wang, Alan C Bovik, Hamid R Sheikh, and Eero P Simoncelli. Image quality assessment: from error visibility to structural similarity. *IEEE TIP*, 13(4):600–612, 2004. [9](#)
- [68] Ke Xian, Chunhua Shen, Zhiguo Cao, Hao Lu, Yang Xiao, Rui-bo Li, and Zhenbo Luo. Monocular relative depth perception with web stereo data supervision. In *CVPR*, pages 311–320, 2018. [2](#)
- [69] Ke Xian, Jianming Zhang, Oliver Wang, Long Mai, Zhe Lin, and Zhiguo Cao. Structure-guided ranking loss for single image depth prediction. In *CVPR*, pages 611–620, 2020. [2](#), [3](#), [7](#)
- [70] Guanglei Yang, Hao Tang, Mingli Ding, Nicu Sebe, and Elisa Ricci. Transformer-based attention networks for continuous pixel-wise prediction. In *ICCV*, pages 16269–16279, 2021. [2](#)
- [71] Lihe Yang, Bingyi Kang, Zilong Huang, Xiaogang Xu, Jiashi Feng, and Hengshuang Zhao. Depth anything: Unleashing the power of large-scale unlabeled data. *arXiv preprint arXiv:2401.10891*, 2024. [1](#), [2](#), [3](#), [4](#), [7](#), [9](#)
- [72] Lihe Yang, Bingyi Kang, Zilong Huang, Zhen Zhao, Xiaogang Xu, Jiashi Feng, and Hengshuang Zhao. Depth anything v2. *arXiv preprint arXiv:2406.09414*, 2024. [1](#), [2](#), [4](#), [6](#)
- [73] Chandan Yeshwanth, Yueh-Cheng Liu, Matthias Nießner, and Angela Dai. Scannet++: A high-fidelity dataset of 3d indoor scenes. In *ICCV*, pages 12–22, 2023. [2](#), [9](#)
- [74] Lvmin Zhang, Anyi Rao, and Maneesh Agrawala. Adding conditional control to text-to-image diffusion models. In *ICCV*, pages 3836–3847, 2023. [1](#)
- [75] Shanshan Zhao, Huan Fu, Mingming Gong, and Dacheng Tao. Geometry-aware symmetric domain adaptation for monocular depth estimation. In *CVPR*, pages 9788–9798, 2019. [3](#)
- [76] Zixiang Zhao, Jianshe Zhang, Shuang Xu, Zudi Lin, and Hanspeter Pfister. Discrete cosine transform network for guided depth map super-resolution. In *CVPR*, pages 5697–5707, 2022. [3](#)
- [77] Chuanxia Zheng, Tat-Jen Cham, and Jianfei Cai. T2net: Synthetic-to-realistic translation for solving single-image depth estimation tasks. In *ECCV*, pages 767–783, 2018. [3](#)
- [78] Zhiwei Zhong, Xianming Liu, Junjun Jiang, Debin Zhao, and Xiangyang Ji. Guided depth map super-resolution: A survey. *ACM Computing Surveys*, 2023. [3](#)